

# *In-situ* atomic force microscopic study of reverse pulse plated Cu/Co-Ni-Cu films

D. GUPTA, A. C. NAYAK, J. MAZHER, R. SENGAR  
*Department of Physics, Bhopal University, Bhopal (M.P.)-462026, India*

K. P. JOSHI  
*Department of Physics, Indore University, Indore (M.P.)-452001, India*

R. K. PANDEY\*  
*Department of Physics, Bhopal University, Bhopal (M.P.)-462026, India*  
*E-mail: ipebu@sancharnet.in*

Cu/Co-Ni-Cu films have been electrochemically synthesized in a single bath using a pulse deposition technique. The results of cyclic voltammetry investigation of the electrodeposition process have been used to optimise bath composition and pulse deposition parameters. The results of *in-situ* examination of the surface morphology using Atomic Force Microscopy (AFM) have been presented to show reduction in surface roughness following pulse deposition. Pulse plated multilayers of Cu/Co-Ni-Cu have also been characterised using Glancing Angle X-ray Diffraction (GAXRD) studies.

© 2004 Kluwer Academic Publishers

## 1. Introduction

The electrochemical routes of deposition of the metallic layers are of considerable technological interest due to their unique capability to fabricate extremely small and complex three dimensional structure with high throughput, relatively inexpensively [1–5]. Recently, application of electrodeposition for growth of compositionally modulated alloys and multilayers has also been reported [6–13]. In order to achieve control over surface and interface roughness of the electrodeposits, we have carried out *in-situ* atomic force microscopy studies during pulse plating of Cu and Co-Ni-Cu films. Our preliminary results have been presented in this report.

## 2. Experimental details

The schematic diagram of the electrochemical workstation has been shown in Fig. 1. A standard three-electrode geometry consisting of a copper foil cathode (as substrate), platinum counter electrode and saturated calomel reference electrode (SCE) was employed during all electrodeposition experiments. The working and counter electrodes were vertically held in position using teflon seals and screw thread joints in a glass cell with multiple entry ports. The standard electrodeposition bath was prepared by dissolving  $\text{CoSO}_4 \cdot 7\text{H}_2\text{O}$  (140.0 g/l),  $\text{NiCl}_2$  (4.6 g/l), Boric Acid (28.1 g/l) and  $\text{CuSO}_4 \cdot 5\text{H}_2\text{O}$  (1.2 g/l) in triple distilled water at pH 2.1. For growth of Cu/Co-Ni-Cu multilayers, 28.0 g/l  $\text{NiSO}_4 \cdot 6\text{H}_2\text{O}$  was also added in the standard bath. All the reagents were of AR grade from Emerck. The mass transport rate of ions was continuously controlled

by recirculating fresh electrolyte from a reservoir using a peristaltic pump. An EG&G potentiostat/galvanostat modulated by a specially designed electronic circuit provided the necessary potentiostatic pulse waveform for electrodeposition. The circuit could be programmed to provide variable duty cycle potentiostatic pulses with a preselected frequency for a given time interval.

For initial optimization of the deposition parameters, steady state cathodic polarization and cyclic voltammetry experiments were carried out on the indium tin oxide coated glass substrates. However, all other electrodeposition experiments were performed using cold rolled copper foils as substrate. Prior to deposition, the substrate was polished to 0.3 micron finish using alumina powder and then washed in Extron (Emerck). This was followed by boiling in  $\text{CCl}_4$  and agitation in ultrasonic cleaner. Just prior to deposition, the substrate surface was etched electrochemically in dilute  $\text{H}_2\text{SO}_4$  to remove any surface oxide and rinsed thoroughly in distilled water. The cold rolled Cu foil had a preferred (111) orientation, which was further enhanced by electrodeposition of approximately 50 nm thick copper film. Potentiostatic pulses of height  $-0.2$  V and  $-1.0$  V were used for electrodeposition of Cu and Co-Ni-Cu layers respectively. The typical frequencies and duty cycles employed for the deposition of Cu & Co-Ni-Cu were 200 Hz, 60% & 400 Hz, 80% respectively. For the deposition of alternate layers of Cu & Co-Ni-Cu, the deposition programmes were alternatively triggered for 23.5 ( $T_3$ ) and 2 ( $T_1$ ) seconds respectively. Fig. 2 represents a typical potentiostatic pulse profile employed in the electrodeposition runs. Note that a delay time  $T_2$

\* Author to whom all correspondence should be addressed.

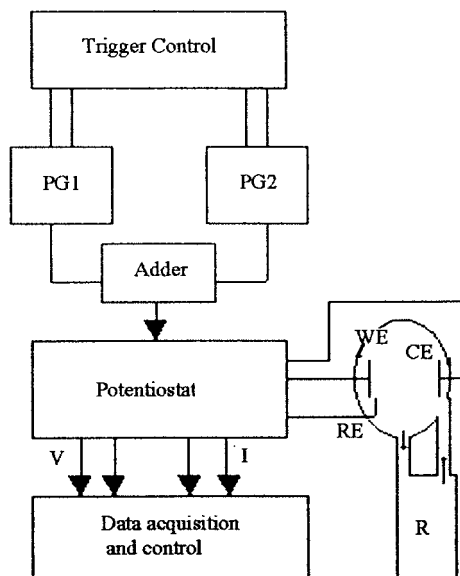


Figure 1 Schematic diagram of the electrodeposition arrangement: PG1 and PG2 pulse generators, R-flow control and reservoir, WE, CE & RE represent working, counter and reference electrode respectively.

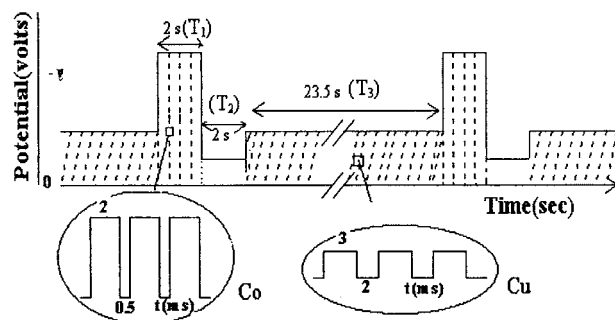


Figure 2 Schematic diagram of the potentiostatic pulses used for electrodeposition of multilayers.  $T_1$  and  $T_3$  represent the triggers employed for electrodeposition of Co-Ni-Cu and Cu respectively. The insets show the pulse profile employed during  $T_1$  &  $T_3$ .

of 2 s was deliberately introduced between  $T_1$  and  $T_3$  to allow the interfacial concentrations to attain equilibrium. The nominal thicknesses of Cu & Co-Ni-Cu layers following the deposition duration of  $T_3$  &  $T_1$  seconds as determined by X-ray reflectivity data were 2.2 and 2.8 nm respectively.

Deposit morphology was studied *in-situ* using an atomic force microscope (AFM) (Shimadzu multimode wet SPM 9500J2, Japan). A  $125 \mu\text{m} \times 125 \mu\text{m}$  peizo-scanner with vertical  $z$ -axis resolution of 0.1 nm was employed for surface scan. Imaging was carried out using 20 nm wide legged silicon nitride cantilevers (spring contrast 1.2 N/m) in contact mode with reported contact force of the order of 1 nN. Before scanning, the condition of the cantilever was cross examined by recording the images of a freshly cleaved mica surface.

The microstructure of the electrodeposited multilayers was investigated with the help of a Shimadzu, Japan X-ray diffractometer (XRD 6000). For this purpose, glancing angle X-ray diffraction pattern (GAXRD) were recorded between  $2\theta$  interval of  $40^\circ$  to  $55^\circ$  and a fixed angle of incidence of  $0.5^\circ$ . A 0.05 mm divergence slit was employed to reduce the beam divergence. A graphite monochromator placed on the de-

tor side was used to filter the Cu  $k_\beta$  radiation. Data were recorded using continuous scan @  $1^\circ$  per min.

### 3. Results and discussions

The cathodic depositions of Cu, Co & Ni have been widely studied by several researchers [14–17]. The standard reduction potentials for the three elements can be expressed in the order of their nobility as  $E_{\text{Cu}}(-0.09) > E_{\text{Ni}}(-0.49) > E_{\text{Co}}(-0.52)$ . However, cobalt and nickel exhibit anomalous co-deposition behavior [18] so that the deposition of nickel is inhibited in presence of cobalt. In order to understand the various electrochemical processes in the plating bath used in the present studies, slow scan cyclic voltammograms were recorded at a scan rate of 2 mV/s in the standard bath containing 28 g/l(S1); 31 g/l (S2); and 34 g/l (S3)  $\text{NiSO}_4 \cdot 6\text{H}_2\text{O}$ . A typical cyclic voltammogram recorded in bath  $S_1$  has been shown in Fig. 3. The cathodic & anodic peak positions recorded in the cyclic voltammogram have been summarized in Table I. The forward cathodic sweep exhibited an onset at  $-0.15$  V corresponding to the reduction of the copper ions. As the substrate potential was continuously ramped to more negative values, the cathodic current approached a limiting value due to the diffusion-controlled deposition of copper. The value of the limiting current density was  $0.23 \text{ mA/cm}^2$  for the

TABLE I The positions of peak potentials and peak currents observed following increase in the  $\text{NiSO}_4 \cdot 5\text{H}_2\text{O}$  concentration in the plating bath.  $S_1$ ,  $S_2$ ,  $S_3$  refer to three bath compositions (see text)

Electrochemical process	Peak position (volts vs. SCE)	Peak current density ( $\text{mA/cm}^2$ )		
		S1	S2	S3
Deposition of Cu	-0.15	-0.23	-0.39	-0.39
Deposition of Cobalt oxide	-0.66	-2.20	-2.73	-2.34
Deposition of elemental Co	-0.81	-3.12	-3.12	-3.28
Formation of hydroxide phase of Co [18]	-0.37	+1.95	+1.33	+1.25
Dissolution of Co	-0.11	+3.36	+2.73	+2.57
Dissolution of Ni	+0.01	+3.83	+3.75	+3.82

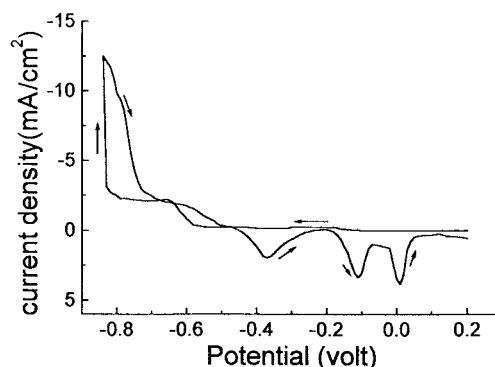
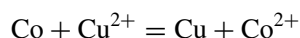


Figure 3 A typical voltammogram recorded on a copper foil working electrode using a ramp rate of 2 mV/s in an electrolyte containing 140 g/l  $\text{CoSO}_4 \cdot 7\text{H}_2\text{O}$ , 28 g/l  $\text{NiSO}_4 \cdot 6\text{H}_2\text{O}$ , 4.6 g/l  $\text{NiCl}_2$ , 28.1 g/l Boric acid, and 1.4 g/l  $\text{CuSO}_4 \cdot 5\text{H}_2\text{O}$  (bath  $S_1$ ).

concentrations employed in this investigation. Beyond  $-0.57$  V the cathodic current registered a rise once again exhibiting a shoulder at  $-0.66$  V & subsequently attaining a plateau up to  $-0.79$  V. The occurrence of a new onset at  $-0.57$  V implied existence of a new cathodic process. This cathodic peak was also recorded even in the absence of the nickel ions in the bath. It was, therefore, concluded that the new cathodic on set at  $-0.57$  V is associated with the reduction of cobalt ions at the working electrode.

Jiang *et al.* [19] have also observed a similar cathodic peak at  $-0.6$  V during cyclic voltammetry studies in aqueous  $\text{CoCl}_2$  bath and assigned its origin to the reactive reduction of cobalt in presence of dissolved oxygen. Formation of an oxide of cobalt in this region could, therefore, be a distinct possibility. Indeed, structural characterisation of electrodeposits grown by us at  $-0.65$  V revealed presence of cobalt oxide [20]. The cathodic onset at  $-0.57$  V can, therefore, be unambiguously associated with the growth of a cobalt oxide/suboxide phase. Beyond  $-0.79$  V the cathodic current increased rapidly due to kinetically controlled reduction of cobalt ions and formation of elemental cobalt. Due to the close proximity of the reduction potential of nickel & cobalt and the diffusion limited deposition of copper, formation of Co-Ni-Cu alloy can not be ruled out in this region.

The anodic back sweep exhibited four peaks at  $-0.37$  V;  $-0.11$  V;  $+0.01$  V and  $0.23$  V (not shown in Fig. 3). Since the first two peaks were also seen in the cyclic voltammogramme in aqueous bath containing  $\text{CoCl}_2$  only; these can be assigned to the reverse (anodic) processes involving electrodeposited cobalt. Jiang *et al.* [19] in an earlier report have also assigned the two peaks to formation of  $\text{Co}(\text{OH})_2$  and stripping of cobalt. The third anodic peak at  $-0.01$  V was seen only when nickel ions were present in the electrolyte. It can, therefore, be assigned to Ni stripping. From the Table I, it is obvious that the anodic peak current density corresponding to cobalt dissolution peaks at  $-0.37$  and  $-0.11$  V systematically decreased as the nickel ion concentration in the bath increased. This trend implied increased inhibition of cobalt dissolution in the presence of nickel. Shima *et al.* [21] and Peter *et al.* [22] have also reported dissolution of electrodeposited cobalt in the electrolyte in the presence of copper ions. The dissolution process for cobalt film in the bath can be expressed as,



In the presence of such a dissolution reaction, it is difficult to plate compact layer of cobalt and copper alternately. The co-deposition of nickel along with cobalt, therefore, seems to inhibit the cobalt dissolution process. Finally, the anodic peak at  $+0.23$  V was assigned to stripping of electrodeposited copper.

Typical two and three dimensional images of the polished copper foil as seen *in situ* by atomic force microscope has been shown in Fig. 4a and b. The surface of the foil is marked by formation of deep channels, which might have been caused during polishing. The average

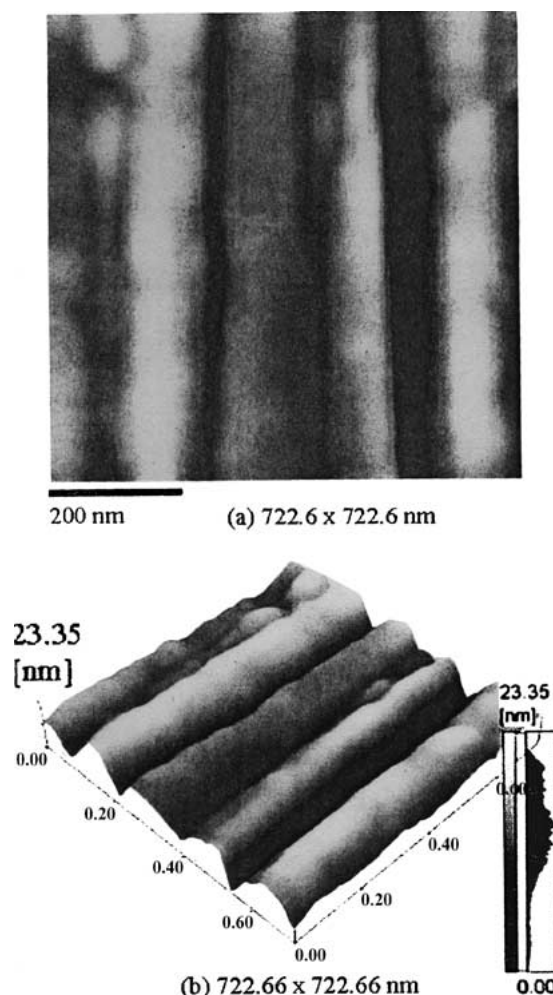
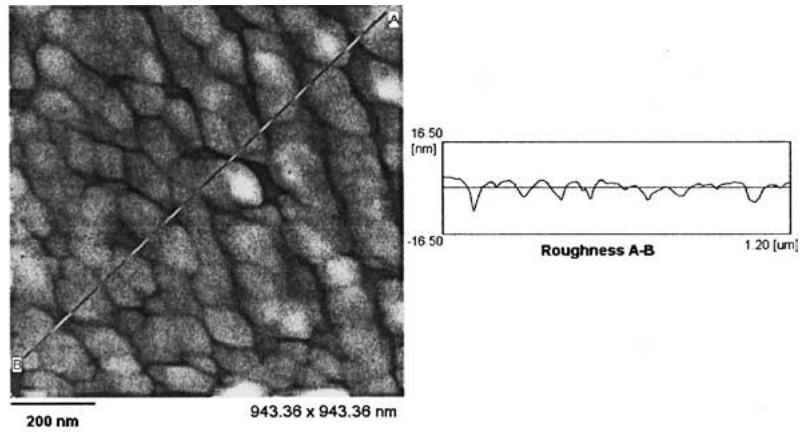
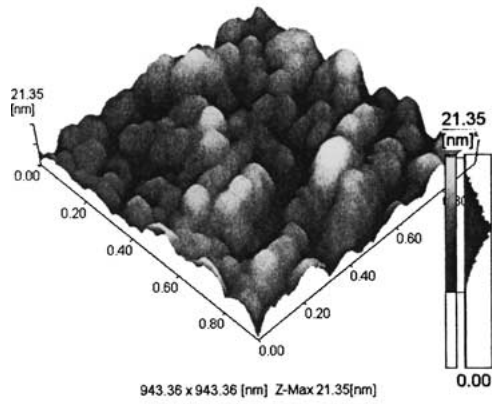


Figure 4 AFM images of a polished copper foil substrate: (a) Top view and (b) 3-D view.

and rms roughness of the substrate were found to be 3.3 nm and 4.3 nm respectively. During dc electrodeposition, one would normally expect that these surface non-uniformities will amplify as the thickness of the electrodeposit increases. However, it can be shown [23] that the amplification of the surface roughness can be considerably controlled by a periodic reverse pulse deposition. In the present study, the pulse waveform employed for the deposition was chosen with this objective. The anodic excursion of the pulse waveform was expected to electrochemically etch out sharp hillocks thereby yielding a smoother surface. To verify our expectation, we employed continuous *in situ* imaging of the surface during electrodeposition. Fig. 5a and b represent typical two and three-dimensional surface morphology of a copper film following 10 s of electrodeposition. A uniform and compact granular growth can be evidenced from the figure. The result of the typical line profile analysis employed for the surface roughness calculation has also been shown in the figure. The average and the rms roughness so obtained were 1.51 and 1.93 nm respectively. The *in-situ* image of the surface of the cobalt film following 2s of electrodeposition has also been shown in Fig. 6a and b. Our AFM results again reveal a compact granular morphology with average and rms roughness values of 1.0 and 1.19 nm respectively. It can, therefore, be concluded from the AFM

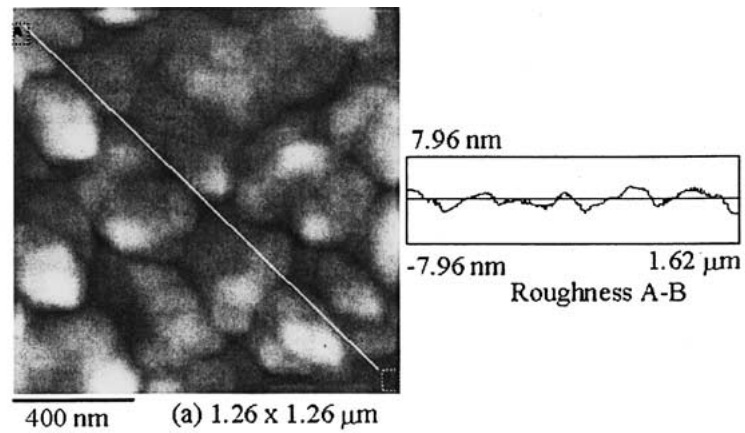


(a)

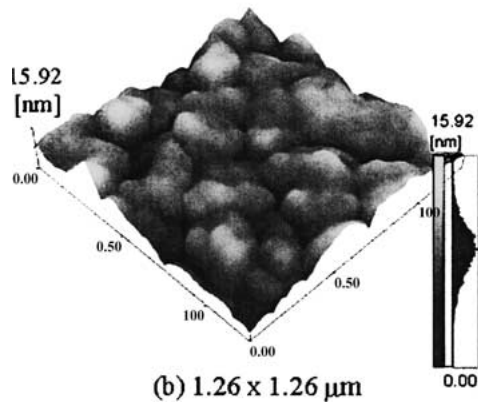


(b)

Figure 5 AFM images and line profile analysis of a typical copper film electrodeposited for 10 s: (a) Top view and (b) 3-D view.



(a) 1.26 x 1.26 μm



(b) 1.26 x 1.26 μm

Figure 6 AFM images and line profile analysis of a typical cobalt film electrodeposited for 2 s: (a) Top view and (b) 3-D Dimensional view.

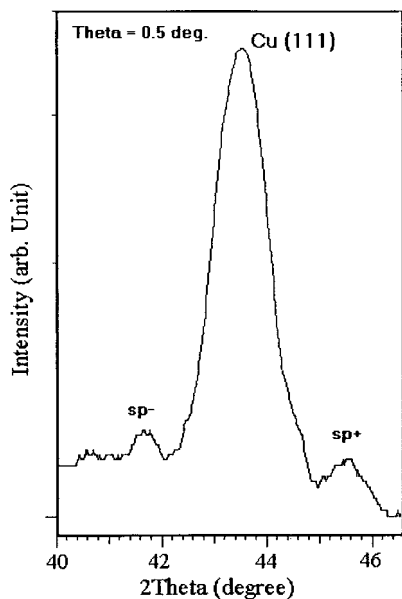


Figure 7 Glancing angle X-ray diffraction pattern of a Cu/Co-Ni-Cu multilayer with 30 bilayer periods.

studies that the pulse deposition cycle employed in the present studies considerably alleviates the problem of surface roughness amplification, yielding a smooth surface morphology.

Glancing angle XRD study was employed to ascertain formation of coherent multilayers of Cu/Co-Ni-Cu using pulse deposition. If bilayer periodicity is retained throughout the multilayer structure, the main Bragg peak will be surrounded by satellite peaks on both sides [24, 25]. The GAXRD data recorded for a sample with 30 bilayer period at a glancing angle of  $0.5^\circ$ , exhibited main Bragg peaks corresponding to (111) and (200) reflection of copper substrate. Fig. 7 shows a typical experimental result recorded between  $2\theta = 40^\circ$  to  $47^\circ$ . The sharp reflex at  $2\theta = 43.48^\circ$  corresponded to the main diffraction peak for (111) planes of copper. The zeroth order main diffraction peak of the Cu/Co-Ni-Cu superlattice can not be resolved from the (111) peak of Cu due to instrumental limitations. The (111) main peak was found to be flanked prominently by the first order satellite peaks. These have been marked as  $sp^-$  &  $sp^+$ . These observations provide evidence of growth of coherent multilayers. The satellite peaks surrounding the main diffraction peak are of weak intensities, indicating that some interlayer mixing at the interface has occurred probably, introducing a non-square wave type composition modulation. Further, it is seen that the satellite peaks surrounding the main diffraction peak are of unequal intensity. Two factors can contribute to this observation viz. change in (a) modulation wavelength  $\Lambda$ , (b) coherent and non-coherent strain modulation present in the layered structure [25–28].

If coherent domain size in multilayer is larger than the modulation wave length, then the bilayer period  $\Lambda$  can be calculated from the satellite peak positions using the following relationship [29]:

$$1/\Lambda = \sin(\theta_n^+) - \sin(\theta_n^-)/n\lambda \quad (1)$$

where  $(\theta_n^+)$  and  $(\theta_n^-)$  are positions of  $n$ th order satellite peaks surrounding the main diffraction peak. The superlattice bilayer period calculated using Equation 1 was  $48.3 \text{ \AA}$ .

#### 4. Conclusion

We have investigated pulse deposition of Cu and Co-Ni-Cu films. Cyclic voltammetry experiments were employed to study the electrochemical process in the plating bath. It was shown that the presence of nickel is helpful in inhibiting dissolution of cobalt during the copper deposition cycle. *In-situ* investigation of the surface morphology using atomic force microscopy indicated a uniform surface coverage. The pulse plating was shown to decrease the surface roughness considerably. The r.m.s. surface roughness of the electrodeposited copper (1.93 nm) and Co-Ni (1.19 nm) were thus found to be lower than that of substrate (4.3 nm). Glancing angle X-ray diffraction studies have shown that coherent multilayers can be grown from the single bath.

#### Acknowledgement

This work was carried out from the research grants received from the Department of Science and Technology Govt. of India, New Delhi and the Special Assistance/COSIST program grant of University Grant Commission, New Delhi. These are gratefully acknowledged.

#### References

1. H. ZAMAN, A. YAMADA, H. FUKUDA and Y. UEDA, *J. Electrochem. Soc.* **145** (1998) 565.
2. A. N. CORREIA and S. A. S. MACHADO, *Electrochim. Acta* **45** (2000) 1733.
3. CHIN-AN CHANG, *Appl. Phys. Lett.* **57** (1990) 297.
4. U. EBELS, J. L. DUVAIL, P. E. WIGEN, L. PIRAUX, L. D. BUDA and K. OUNADJELA, *Phys. Rev. B* **64** (2001) 144421-1.
5. GYANA R. PATTANAİK, DINESH K. PANDYA and SUBHASH C. KASHYAP, *J. Electrochem. Soc.* **149** (2002) C363.
6. G. NABIYOUNI, O. I. KASYUTICH, S. ROY and W. SCHWARZACHER, *ibid.* **149** (2002) C218.
7. J. YAHALOM and O. ZADOK, *J. Mater. Sci.* **22** (1987) 499.
8. J. J. KELLY, P. E. BRADLEY and D. LANDOLT, *J. Electrochem. Soc.* **147** (2000) 2975.
9. A. CZIRAKI, V. PIERRON-BOHNES, C. ULHAQ-BOUILLET, E. TOTH-KADAR and I. BAKONYI, *Thin Solid Films* **318** (1998) 239.
10. KEITH D. BIRD and M. SCHLESINGER, *J. Electrochem. Soc.* **142** (1995) L65.
11. D. S. LASHMORE and M. P. DARIEL, *ibid.* **135** (1988) 1218.
12. M. ALPER, P. S. APLIN, K. ATTENBOROUGH, D. J. DINGLEY, R. HART, S. J. LANE, D. S. LASHMORE and W. SCHWARZACHER, *J. Magn. Mater.* **126** (1993) 8.
13. M. SHIMA, L. SALAMANCA-RIBA, T. P. MOFFAT, R. D. MCMICHAEL and L. J. SWARTZENDRUBER, *J. Appl. Phys.* **84** (1998) 1504.
14. KEITH Y. SASAKI and JAN B. TALBOT, *J. Electrochem. Soc.* **145** (1998) 981.
15. JEAN HORKANS, I-CHIA HSU CHANG, P. C. ANDRICACOS and ELIZABETH J. PODLAHA, *ibid.* **138** (1991) 411.

16. T. COHEN-HYAMS, W. D. KAPLAN, D. AURBACH, Y. S. COHEN and J. YAHALOM, *ibid.* **150** (2003) C-28.
17. Q. HUANG, D. P. YOUNG, J. Y. CHAN, J. JIANG and E. J. PODLAHA, *ibid.* **149** (2002) C-349.
18. N. ZECH, E. J. PODLAHA and D. LANDOLT, *ibid.* **146** (1999) 2886.
19. S. P. JIANG and A. C. C. TSEUNG, *ibid.* **137** (1990) 3381.
20. DHIRENDRA GUPTA, A. NAYAK, D. KOUSIK, S. K. KULKARNI and R. K. PANDEY (to be published).
21. M. SHIMA, L. SALAMANCA-RIBA and T. P. MOFFAT, *Electrochem. Solid State Lett.* **2** (1999) 271.
22. L. PETER, A. CZIRAKI, L. POGANY, Z. KUPAY, I. BAKONYI, M. UHLEMANN, M. HERRICH, B. ARNOLD, T. BAUER and K. WETZIG, *J. Electrochem. Soc.* **148** (2001) C-168.
23. R. K. PANDEY, S. N. SAHU and S. CHANDRA in "Hand Book of Semiconductor Electrodeposition" (Marcel Dekker Inc., New York, 1996) p. 107.
24. TERUYA SHINJO, Surface Science Report (North Holland, 1991) vol. 12, p. 49.
25. M. PIECUCH and L. NEVOT, *Materials Science Forum*, **59/60** (1990) 93.
26. A. WEIDINGER, D. NAGENGAST, CH. REHM, F. KLOSE and B. PIETZA, *Thin Solid Films* **275** (1996) 48.
27. T. BIGAUIT, F. BOCQUET, S. LABAT and O. THOMAS, *Phys. Rev. B* **64** (2001) 125414.
28. PHILIP C. YASHAR and WILLIAM D. SPROUL, *Vacuum* **55** (1999) 179.
29. ERIC E. FULLERTON, IVAN K. SCHULLER, H. VANDERSTRAETEN and BRUYNSEAEDE, *Phys. Rev. B* **45** (1992) 9292.

*Received 8 May  
and accepted 22 October 2003*